Korean J. Chem. Eng., 35(3), 645-653 (2018)
DOI: 10.1007/s11814-017-0343-3

pISSN: 0256-1115
eISSN: 1975-7220

Low-temperature CO oxidation of $Pt/Al_{0.1}Ce_{0.9}O_x$ catalysts: Effects of supports prepared with different precipitants

Jung-Hyun Park*, Hyeryeung Noh, Tae-Sun Chang*, and Chae-Ho Shin**,†**

*Greenhouse Gas Resources Research Group, Korea Research Institute of Chemical Technology, Daejeon 34114, Korea
**Department of Chemical Engineering, Chungbuk National University, Cheongju, Chungbuk 28644, Korea
(*Received 28 August 2017 • accepted 12 December 2017*)

Abstract−We prepared 0.1Al-0.9Ce supports using various precipitants such as NH_4OH, KOH, NaOH, K_2CO_3, and Na_2CO_3 to prepare Pt-based CO oxidation catalysts. Of the studied catalysts, the Pt/0.1Al-0.9Ce_NH_4OH catalyst showed the optimum activity for CO oxidation. Catalysts prepared with carbonate-form precipitants revealed relatively lower activity than carbonate-free precipitants. A temperature at 50% CO conversion of all samples was observed in the low-temperature region in the presence of water vapor because of the promotional effect of the water-gas shift reaction. Several characterization results revealed that catalytic activity was related to oxygen capacity and Pt dispersion was attributable to precipitant nature.

Keywords: Pt/0.1Al-0.9Ce Catalyst, Precipitants, Anion, Pt Dispersion, Oxygen Vacancy

INTRODUCTION

Carbon monoxide (CO), a colorless, odorless, and toxic air pollutant, is produced mainly via incomplete combustion of carbon-containing materials. Approximately 90% of CO is derived from vehicle emissions [1], and most CO is released under the "cold-start" conditions of an engine, when the catalytic converter has an insufficient operating temperature [2,3]. If the CO oxidation catalysts are effective at low-temperature operating conditions, the cold-start problem associated with automotive vehicle engines can be overcome [4].

Catalysts based on noble metals (e.g., Pt, Pd, Rh, Au, and Ru) are generally used in the oxidation of CO because of their excellent catalytic activity [5-11]. However, such catalysts have to be supported on various oxides (e.g., Al_2O_3, SiO_2, FeO_x, ZrO_2, and CeO_2) because of their poor mechanical and thermal properties [12-17]. In particular, a CeO_2-based catalyst has been studied widely as an additive or support in various catalysis fields. This oxide has unique properties of oxygen storage capacity (OSC) that result from the oxidation state of Ce^{3+}/Ce^{4+} and high oxygen mobility in the ceria lattice [6,18]. Despite these advantages, the drawbacks of poor thermal stability and deactivation of the redox couple limit its commercial applicability [19,20]. However, the formation of composite oxides by substituting another metal component into the CeO_2 lattice can overcome these drawbacks [21]. ZrO_2 is considered a most interesting oxide. The addition of ZrO_2 to CeO_2 enhances their OSC, redox, and thermal properties because of the partial substitution of Ce^{4+} with Zr^{4+} in the CeO_2 lattice. It has been established that the substitution of 25 mol% ZrO_2 in CeO_2 produces the highest OSC activity, which provides excellent catalytic activity in various oxidation reactions [22-24].

The CeO_2-Al_2O_3 oxide system is widely used and one of the most promising oxides for removing air pollutants in automobile exhaust gases [25]. The high thermal stability and reducibility of CeO_2-Al_2O_3 oxides make them attractive supports for metal catalysts. Chen et al. [26] reported that a Pt catalyst on a 15%CeO_2-Al_2O_3 support showed 100% conversion of CH_2Cl_2 oxidation at 400 °C. They found that Pt on CeO_2 dispersed on Al_2O_3 had higher OSC activity than that of Pt/CeO_2 or Pt/Al_2O_3 [27]. We also studied the effects of Al addition into the CeO_2 support for a Pt catalyst in CO oxidation [28]. The Pt/AlCe catalyst with an Al/Ce molar ratio of 0.1/0.9 exhibited superior catalytic activity for CO oxidation compared with that of Pt catalysts supported on different molar ratio of Al-Ce oxides.

The catalytic and structural properties of a catalyst affect various factors, including the nature of the support, active metal precursors, preparation method, heat treatment history, and reaction conditions [29-32]. Tang et al. [30] reported that a Pt/MnO_x-CeO_2 catalyst, prepared using chlorine-free Pt precursor, showed high catalytic activity and stability in the complete oxidation of formaldehyde. A silicotungstic acid doped CeO_2 catalyst, prepared using ammonia solution as a precipitant, was found to exhibit superior catalytic activity in selective catalytic reduction on NO_x by NH_3 [33]. The catalytic activity for CO oxidation of copper-manganese oxides depends strongly on the employed precipitants and precursors, and a combination of an acetate precursor of copper and manganese and a carbonate precipitant was found to produce superior catalytic activity [34]. In this regard, we studied the effects of precipitants on 0.1Al-0.9Ce mixed oxide, which was found to have good catalytic properties for CO oxidation [28].

In the present study, we prepared the 0.1Al-0.9Ce catalyst with various precipitants, e.g., ammonium hydroxide (NH_4OH), sodium hydroxide (NaOH), potassium hydroxide (KOH), potassium carbonate (K_2CO_3), and sodium carbonate (Na_2CO_3), and used them

†To whom correspondence should be addressed.
E-mail: chshin@chungbuk.ac.kr

as supports for Pt-based catalysts. Various characterization tools were used to determine the physicochemical properties of the catalysts. The information derived from these analyses was correlated with CO oxidation activity.

EXPERIMENTAL

1. Catalyst Preparation

All chemicals were analytical grade and used as received without further purification. The 0.1Al-0.9Ce oxide support was prepared using the precipitation method with different precipitants: ammonia solution (NH_4OH (AH), Samchun, 28%-30%), potassium hydroxide (KOH (PH), Samchun, 95%), sodium hydroxide (NaOH (SH), Junsei, 99%), potassium carbonate (K_2CO_3 (PC), Duksan, 99%), and sodium carbonate (Na_2CO_3 (SC), Junsei, 99%). For each, 1 M of precipitant solution was added to 300 ml aqueous solution of aluminum nitrate nonahydrate ($Al(NO_3)_3{\cdot}9H_2O$, Junsei, 98%) and cerium nitrate hexahydrate ($Ce(NO_3)_2{\cdot}6H_2O$, Samchun, 99%) until the pH of the solution reached 10. The resulting solution was aged at 70 °C for 24 h, filtered, and washed several times with de-ionized water. The filtered cake was dried at 100 °C for 12 h and then calcined at 500 °C for 2 h in flowing air. The prepared samples were designated by AlCe-X, where X represents the abbreviation of the precipitant.

The 1 wt% Pt/0.1Al-0.9Ce catalysts were prepared by the incipient wetness impregnation method using an aqueous solution of $Pt(NH_3)_4(NO_3)_2$ (Aldrich, 99%). The catalyst was dried at 30 °C for 12 h and then calcined at 500 °C for 2 h under flowing air.

2. Catalyst Characterization

The crystalline structure of the catalyst was analyzed using a Siemens D5005 diffractometer with CuK_α radiation operating at 30 kV and 50 mA with a scanning rate of 0.4° min^{-1}. Phases were identified by matching the experimental patterns to the JCPDS powder diffraction file (CeO_2, #01-081-0792). The Brunauer-Emmett-Teller (BET) surface area was measured by N_2 sorption at the liquid nitrogen temperature of −196 °C using a Micromeritics ASAP 2020 instrument. Prior to the measurement, each sample was degassed for 4 h under vacuum at 250 °C. The BET method was used to determine the surface area, and the Barrett, Joyner, and Halenda (BJH) method was used to determine the pore size distribution of the catalysts using desorption isotherms. The morphology and the crystal shape of the prepared catalyst particles were examined by scanning electron microscopy (SEM) using a Hitachi S-2500C scanning electron microscope at an acceleration voltage of 5 kV.

The ^{27}Al MAS NMR spectra were obtained on a Bruker AVANCE 500 spectrometer, at the ^{27}Al frequency of 130.325 MHz, in a 4 mm rotor at a spinning rate of 10.0 kHz. The spectra were obtained with the acquisition of approximately 3000 pulse transients, which were reported with a $\pi/4$ rad pulse length of 1.50 ms and a recycle delay of 1.0 s. The ^{27}Al chemical shifts were reported relative to a solution of $Al(H_2O)_6^{3+}$.

Scanning transmission electron microscopy (STEM) and element mapping were performed using a Philips Tecnai F20 microscope operating at 200 kV. In preparation, the samples were put into glass vials containing ethanol and placed in an ultrasonic bath for a couple of minutes to disperse the individual particles. Then, a drop of the resulting suspension was deposited onto a holey-carbon film supported on a copper grid, which was subsequently dried.

Temperature-programmed reduction experiments with CO as a reductant (CO-TPR) were undertaken using a Pfeiffer OmniStar mass spectrometer (MS) as a detector. Before analysis, each sample (0.05 g) was loaded in a quartz reactor (I.D. 12 mm) and pretreated at 300 °C in a He flow (50 $cm^3{\cdot}min^{-1}$) for 1 h. After cooling to room temperature (RT), a flow of 5% CO/N_2 was introduced through the samples and the temperature was increased from RT to 900 °C at a rate of 10 °C·min^{-1}. The mass signals of m/z=2 (H_2), 28 (CO), 18 (H_2O), and 44 (CO_2) were detected by the MS. In the CO_2-TPD experiment, the catalysts were pretreated at 300 °C for 1 h with a He flow (50 $cm^3{\cdot}min^{-1}$). Following this, they were cooled to RT under the same atmosphere and then treated with 100% CO_2 (50 $cm^3{\cdot}min^{-1}$) for 1 h. After adsorption of CO_2, the reactor was flushed for 1 h under a He flow (50 $cm^3{\cdot}min^{-1}$) to remove physisorbed CO_2, then the temperature was increased from RT to 600 °C at a heating rate of 10 °C·min^{-1}.

The chemisorption of H_2 was measured with a Pfeiffer OmniStar MS as a detector, and the gas mixture of 5% H_2/Ar was used as an adsorbate. Prior to pulse chemisorption, all samples were reduced in pure H_2 at a flow rate of 30 $cm^3{\cdot}min^{-1}$ at 400 °C for 1 h. The reduced samples were purged in a He flow (50 $cm^3{\cdot}min^{-1}$) at 400 °C for 0.5 h and then cooled to RT in the same atmosphere. The amount of H_2 in each pulse was 3.6 mmol, which was introduced using a volumetric sample loop of 2 cm^3 using He (30 $cm^3{\cdot}min^{-1}$) as a carrier gas. The pulse was repeated in 7 min intervals until no further gas uptake by the catalyst was observed. A mass signal of m/z=2 (H_2) was detected. Pt dispersion and the active Pt area were calculated from the amount of H_2 chemosorbed assuming a stoichiometric factor of H/Pts=1.

3. Catalytic Testing for CO Oxidation

CO oxidation was performed in a continuous-flow, fixed bed reaction system with U-shaped quartz (I.D. 12 mm) reactor at atmospheric pressure. Each catalyst (0.02 g) with SiC (1 g) as a diluent was loaded into the reactor and pretreated at 400 °C in the H_2 flow for 1 h, prior to the catalytic reaction. The dry feed stream comprised 1 vol% CO, 4 vol% O_2 and 95 vol% N_2 at a total flow rate of 200 $cm^3{\cdot}min^{-1}$, which was heated at a rate of 4 °C·min^{-1} from 30 to 250 °C. In addition, to examine the effects of H_2O vapor, 3% H_2O vapor was introduced continuously in the reactor through the saturator. The conversion of CO in the reaction was calculated in terms of its percentage consumed. The concentration of CO in the product stream was measured every second using an on-line CO analyzer (TELEDYNE Instrument Analyzer of IR-ways).

RESULTS AND DISCUSSION

Fig. 1 shows the CO conversion profiles of the Pt/AlCe-X catalysts in the absence/presence of water vapor. Prior to the reaction on the Pt/AlCe-X catalysts, the AlCe oxides were tested; however, no noticeable catalytic activity was observed for CO oxidation within the investigated temperature range (not shown). Although all the catalysts achieved 100% CO conversion at temperature <200 °C, the nature of the precipitants had considerable effect the

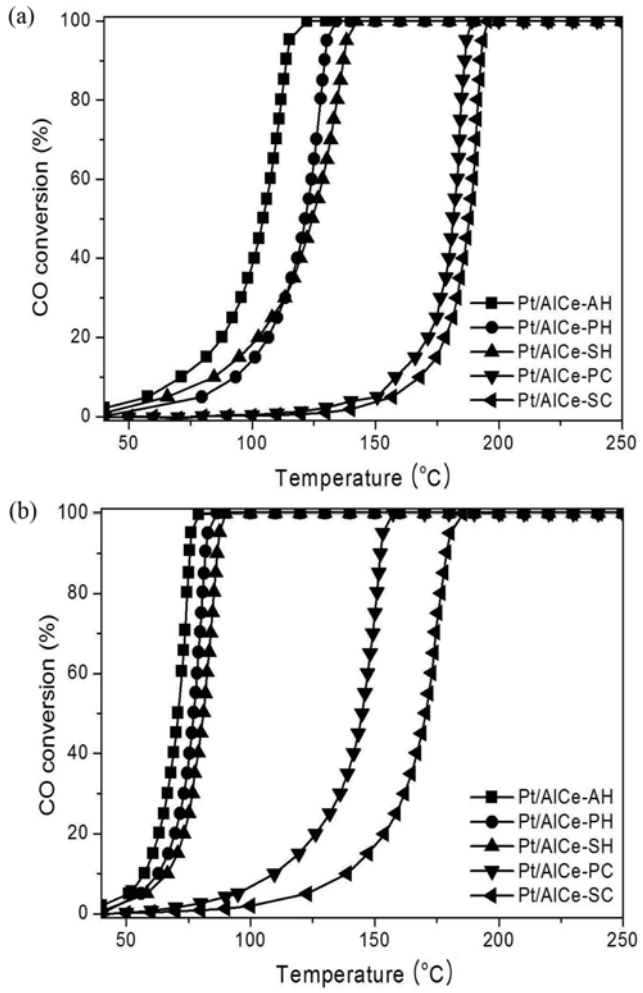

Fig. 1. CO conversion profiles of the Pt/AlCe-X catalysts as a function of reaction temperature: (a) dry conditions: 0.02 g catalyst with 1 g SiC, $CO/O_2/N_2$ (vol%)=1/4/95, total flow rate= 200 cm^3 min^{-1}, and (b) continuous addition of 3% H_2O.

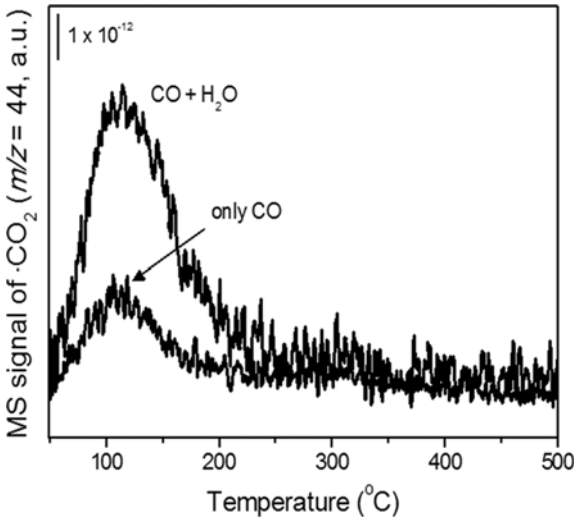

Fig. 2. CO_2 formation profiles of the Pt/AlCe-AH catalyst during CO-TPD after the adsorption of CO only, and CO+H_2O co-adsorption.

catalytic activity for CO oxidation. The Pt/AlCe catalyst prepared by NH_4OH revealed superior CO oxidation activity, for a temperature at 50% CO conversion ($T_{50\%}$) of 104 °C. When the hydroxide-form alkali precipitants (e.g., KOH and NaOH) were used during the preparation of the AlCe oxide, the corresponding catalysts also showed good catalytic activity. However, when the carbonate-form alkali precipitants (e.g., K_2CO_3 and Na_2CO_3) were employed for preparing the AlCe oxides, the catalysts revealed relatively low catalytic activity. The $T_{50\%}$ under reaction conditions in the absence of water vapor increased in the following order: Pt/AlCe-AH<Pt/AlCe-PH<Pt/AlCe-SH<Pt/AlCe-PC<Pt/AlCe-SC.

To investigate the effects of water vapor on catalyst activity, 3% water vapor was introduced simultaneously to the catalyst bed. The light-off curves obtained during the reaction with water vapor are shown in Fig. 1(b). Under wet conditions (water vapor present in the reactant stream), the light-off temperatures were shifted to lower regions ($T_{50\%}$ decreased by about 30 °C) compared with dry conditions (absence of water vapor). There could be several reasons for the increased catalytic activity in the presence of water vapor. One is that the water promotes the water-gas shift (WGS) reaction, which in turn means more CO is converted into CO_2. The second is that the hydroxyl groups formed on the catalyst surface act as a better oxidant than oxygen [35-38]. To investigate the reason for the enhanced catalytic activity in the presence of water vapor, we considered the promotional effects of the WGS. The CO-TPD was performed on the Pt/AlCe-AH catalyst after either adsorption of CO only or co-adsorption of CO and H_2O, as shown in Fig. 2. For the former, CO_2 was produced from the reaction of adsorbed CO on Pt sites and oxygen species of the AlCe oxide. The peak CO_2 desorption after co-adsorption of CO and H_2O was much larger than after CO adsorption only. During the CO-TPD analysis, an equimolar of CO gas introduced into the catalyst bed meant that CO could have been adsorbed on the active sites of the Pt. Thus, the additional water molecules could have been adsorbed as hydroxyl forms on the catalyst surface, which could have affected the CO transition dipole moment. Consequently, formate species (COOH complex) might have formed on the catalyst surface via interaction between CO molecules and H_2O. This complex could have affected the rate of CO oxidation [39]. Therefore, the increased catalytic activity in the presence of water vapor could be attributed to the promotional effect of formate species formed by reaction between the CO and oxygen species [38].

The results of reproducibility tests performed for the Pt/AlCe-AH catalyst, which demonstrated the optimum catalytic activity in CO oxidation, are shown in Fig. 3. The reactions were repeated three times in the absence of water vapor. Fig. 3 shows that complete CO conversion for each run was achieved below 150 °C; however, the temperature of CO conversion shifted to higher regions during the repeated reactions. The decrease in catalytic activity was attributed to a reduction in active sites to oxidation of the Pt species. After the third runs, the used catalyst was treated under the same pretreatment conditions as the reaction and re-tested for CO oxidation. However, the catalytic activity was not recovered completely to that of the first run. The decrease in catalytic activ-

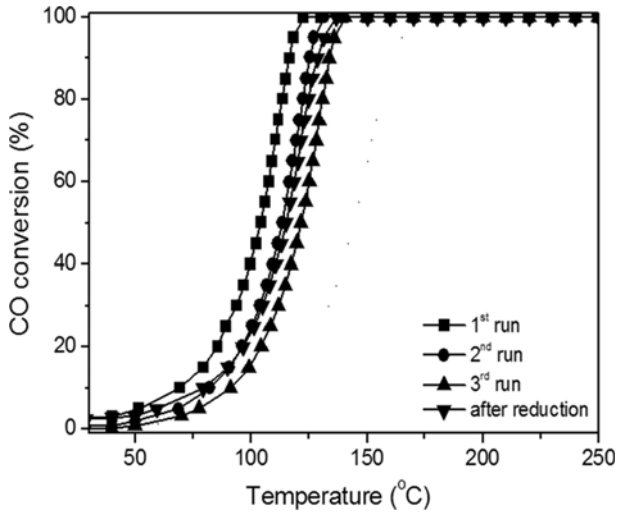

Fig. 3. Reproducibility test for CO oxidation of the Pt/AlCe-AH catalyst under dry reaction conditions. Reaction conditions: 0.02 g catalyst with 1 g SiC, $CO/O_2/N_2$ (vol%)=1/4/95, and total flow rate=200 cm^3 min^{-1}.

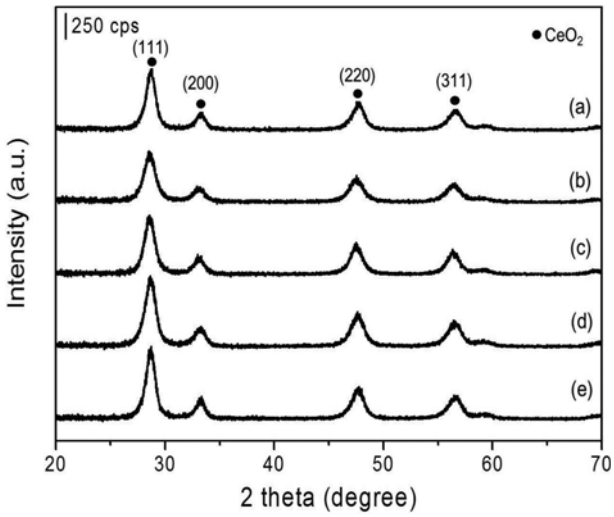

Fig. 4. XRD patterns of the Pt/AlCe-X catalysts: (a) X=AH, (b) PH, (c) SH, (d) PC, and (e) SC.

ity was considered related not only to the oxidation of active Pt specie, but also to other factors, such as the formation of inactive Pt species caused by strong interaction with CO molecules, or Pt metal sintering.

The X-ray diffraction (XRD) patterns and crystallite size of the Pt/AlCe-X catalysts are shown in Fig. 4 and Table 1. The main peaks of the CeO_2 phase were detected on all samples; however, peaks of the PtO_x and Al_2O_3 phases were not observed. This indi-

Table 1. Physicochemical properties of AlCe oxide supports and Pt/AlCe-X catalysts

Sample	Crystallite size (nm)[a]	S_{BET} ($m^2 \cdot g^{-1}$)	Pore volume ($cm^3 \cdot g^{-1}$)	Al/Ce molar ratio	Element contents (wt%)[c]	
					Na	K
Pt/AlCe-AH	10.9	102 (108)[b]	0.272	0.08		
Pt/AlCe-PH	10.5	110 (124)	0.211	0.09		2.0
Pt/AlCe-SH	10.7	104 (109)	0.219	0.09	1.8	
Pt/AlCe-PC	10.8	58 (69)	0.367	0.09		0.4
Pt/AlCe-SC	11.0	17 (26)	0.103	0.08	3.5	-

[a]Calculated from line broadening of the CeO_2 (111) peak, using Scherrer's equation
[b]Values of calcined AlCe oxide support at 500 °C
[c]Determined by EDX analysis

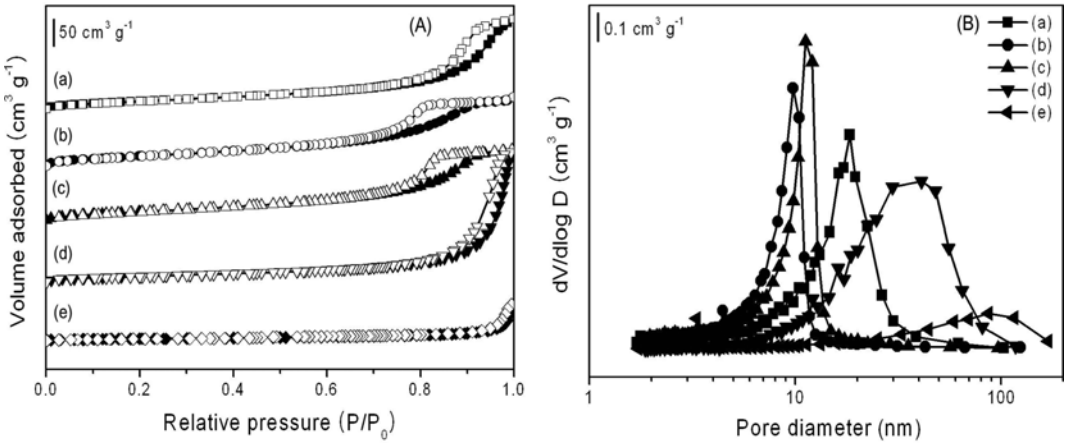

Fig. 5. N_2 sorption isotherms (A) and pore size distribution (B) of the Pt/AlCe-X catalysts; (a) X=AH, (b) PH, (c) SH, (d) PC, and (e) SC.

cates, the PtO_x phase was highly dispersed or that the particles were so small that the signals were not detected by XRD analysis. The crystallite sizes of CeO_2 in the Pt/AlCe-X catalysts showed similar values in the range of 10-15 nm, and distinct differences were not observed with respect to the precipitants.

Table 1 presents the surface areas and total pore volumes of the Pt/AlCe-X catalysts. The catalysts prepared with precipitant that contained hydroxide ions exhibited distinct hysteresis at P/P_o= 0.65-0.90 regions (Fig. 5(A)). Catalysts prepared with hydroxide-form precipitants had higher S_{BET} values (>100 $m^2 \cdot g^{-1}$) compared with those of prepared with precipitants that contained carbonate ions (<60 $m^2 \cdot g^{-1}$). Although the catalysts prepared with hydroxide-form precipitants exhibited small pore sizes, the Pt/AlCe-PC and Pt/AlCe-SC catalysts prepared using carbonate-form precipitants had large pore sizes centered at around 40 and 90 nm, respectively (Fig. 6(B)).

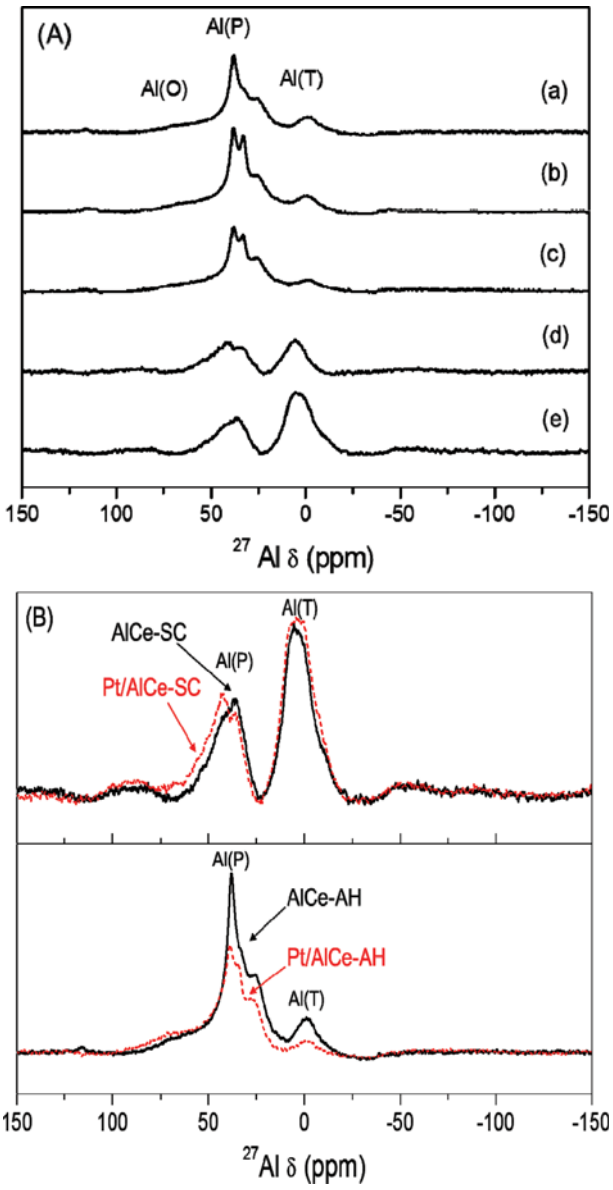

Fig. 6. ^{27}Al MAS NMR spectra of the AlCe-X oxide support (A) and the Pt/AlCe-X catalysts (B); (a) X=AH, (b) PH, (c) SH, (d) PC, and (e) SC.

Fig. 6 shows the ^{27}Al MAS NMR spectra of the AlCe oxides prepared with different precipitants. It is well-known that the NMR spectrum of γ-Al_2O_3 has two peaks at 64.9 and 8.2 ppm that are assigned to tetrahedral and octahedral Al^{3+} ions, respectively [40, 41]. The AlCe oxides showed distinct features compared with pure Al_2O_3. None of the samples showed tetrahedrally coordinated Al^{3+} ions (Al(T)), and the octahedral peak (Al(O)) at ~0 ppm was shifted to a higher field. This indicates that interaction between the Al species and CeO_2 resulted in a distortion of the alumina crystalline structure. In addition, an additional peak at ~38 ppm was observed, consistent with an assignment to penta-coordinated Al^{3+} ions (Al(P)) in the $CeAlO_3$ [41]. As the radius of Al^{3+} ions (0.53 Å) is smaller than that of Ce^{3+} (1.02 Å) and Ce^{4+} (0.97 Å) ions, the Al^{3+} ions can diffuse into the CeO_2 lattice [42]. The peak observed at ~25 ppm was attributed to Al^{3+} that had interacted with Ce^{3+} [43]. The Al(P) peak of the AlCe oxides prepared with hydroxide-form precipitants was more dominant than that of the Al(O), whereas the AlCe oxides prepared with precipitants containing carbonate species showed a relatively small Al(P) peak. In addition, as shown in Fig. 6(B), the peaks of Al(P) and Al(O) for the Pt/AlCe-AH catalyst decreased as compared with the AlCe-AH support. In contrast, the peaks of both AlCe-SC and Pt/AlCe-SC catalysts showed similar values. The carbonate species might hinder the formation of a solid solution between the aluminum and ceria because of strong interaction with metal cations. According to Kwak et al. [44], BaO or Pt species are deposited selectively on the unsaturated penta-coordinated Al^{3+} sites of Al_2O_3 [33,36], and the Pt species that interact on the Al(P) sites are highly dispersed more widely compared with Al(T) or Al(O). These different structural properties might have had an effect on the metal dispersion of the catalysts investigated in this study (Table 2); the hydroxide-form precipitants showed larger Pt dispersion than carbonate precipitants. To understand the effects of the structural properties of Al species on CeO_2, further experiment and analysis are required.

Fig. 7 presents SEM images of AlCe oxides prepared using different precipitants. The average particle sizes of the AlCe oxides were smaller (larger) when hydroxide-form (carbonate-form) precipitants were used. Catalysts prepared with hydroxide-form precipitants showed small-round shapes, whereas those prepared using carbonate-form precipitants were needle-like (K_2CO_3) or rod-like

Table 2. Active Pt metal area, and dispersion of Pt/AlCe-X catalysts

Sample	H_2 uptake (mmol g^{-1})[a]	Active Pt area (m^2 g_{Pt}^{-1})	Pt dispersion (%)[b]
Pt/AlCe-AH	12.3	59.3	24.0
Pt/AlCe-PH	6.6	31.8	12.9
Pt/AlCe-SH	5.2	25.1	10.1
Pt/AlCe-PC	3.4	16.4	6.6
Pt/AlCe-SC	2.9	14.0	5.7

[a]Determined by H_2 pulse chemisorption analysis
[b]Calculated from H_2 uptake assuming stoichiometry of H/Pt_s=1

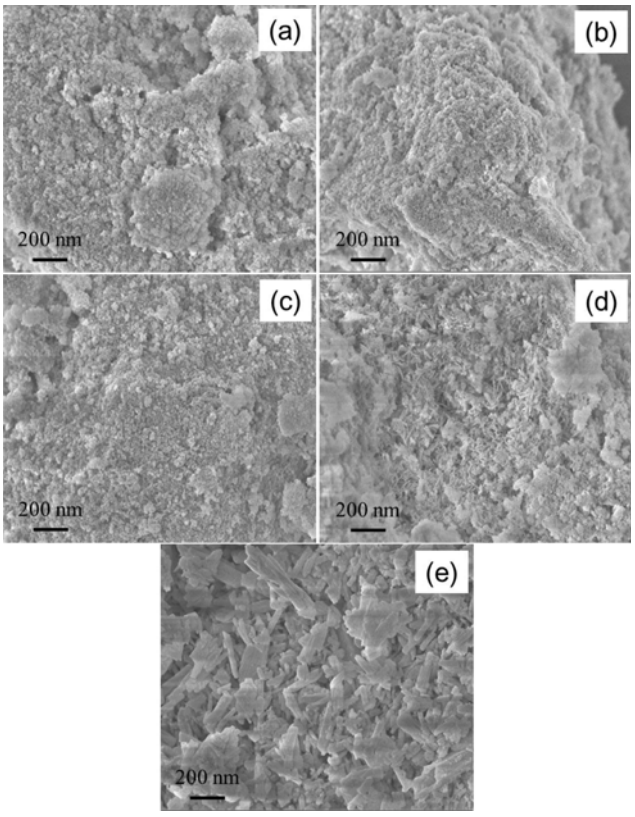

Fig. 7. SEM images of the AlCe-X oxide supports; (a) X=AH, (b) PH, (c) SH, (d) PC, and (e) SC.

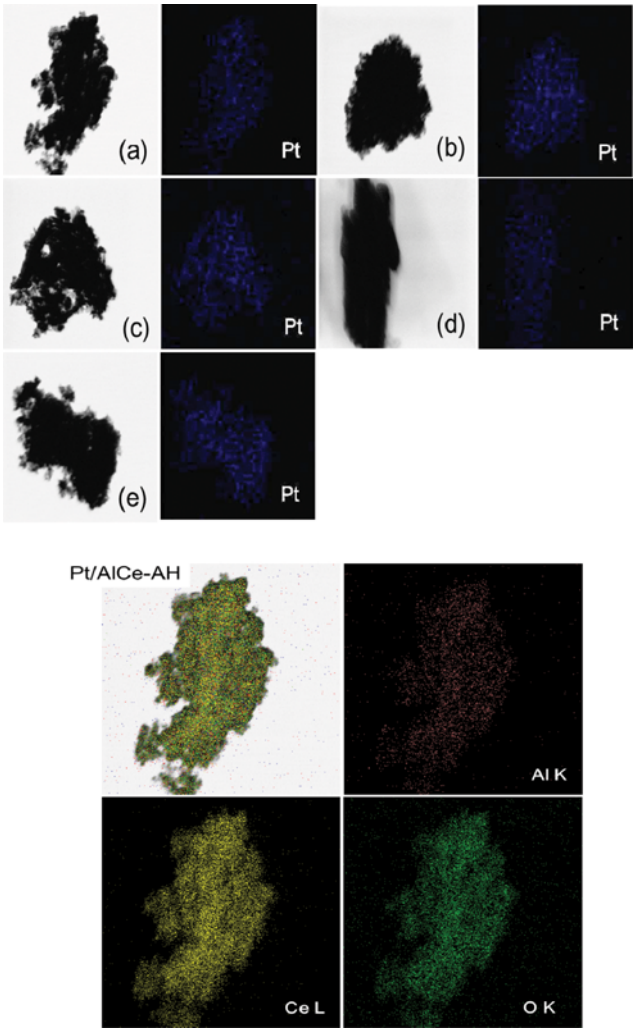

Fig. 8. STEM images and element mapping of the Pt/AlCe-X catayst: (a) X=AH, (b) PH, (c) SH, (d) PC, and (e) SC. The red, yellow, and green colors indicate Al, Ce, and O species, respectively.

(Na_2CO_3) shapes. In addition, the catalyst prepared with K_2CO_3 had particles with irregular shapes, and the particle size was smaller than that of the catalyst prepared with Na_2CO_3. These results indicate that carbonate-form precipitants affect the morphologies of the catalysts during the co-precipitation step and they might alter the catalytic activity for CO oxidation. According to the Pourbaix diagram, during the preparation of the supports, the Al species are precipitated first followed by the Ce species. The rates of precipitation of the Al and Ce species could affect the morphology and surface property of the prepared AlCe supports. Thus, the different morphology observed by the SEM analysis resulted from the different rates of precipitation of the Al and Ce species that depended on the different natures of the precipitants. Fig. 8 shows the STEM and elemental mapping of the Pt/AlCe-X catalysts. All elements of the catalysts were well scattered on the particle; however, here, we showed only the Pt/AlCe-AH catalyst (Fig. 8). Despite the low Al content, the Al atoms are shown well dispersed on the CeO_2 in the images. Small amounts of alkali species were observed in the catalysts prepared with an alkali solution. Table 1 shows the Al/Ce ratio, and the concentrations of Na and K for all catalysts. The Al/Ce molar ratio in the range 0.08-0.09 almost approached a nominal value of 0.11 in the precipitated solution. The concentration of residual alkali metals of 0.4-3.5 wt% was found dependent on the precipitant employed.

The Pt dispersion in the Pt/AlCe-X catalysts was estimated using H_2-pulse chemisorption. Table 2 shows the active Pt area and the Pt dispersion of the Pt/AlCe-X catalysts. The Pt/AlCe-AH catalyst had the highest dispersion (24.0%) in comparison with the other catalysts, and the Pt/AlCe-SC catalyst had the lowest value (5.7%). Although the addition of alkali metals (K or Na) leads to a decrease in metal dispersion [45], in our system, the Pt dispersion of the Pt/AlCe-PH catalyst with 2 wt% K was higher than the Pt/AlCe-PC catalyst with 0.4 wt% K. This indicates various parameters affect metal dispersion and that the type of anions could have a greater effect than the type of cations in determining Pt dispersion. The dispersion of a CeO_2-based catalyst could be overestimated because of the large OSC of the oxide. In addition, the reducible nature of CeO_2 could encapsulate the Pt particles during pretreatment under a flow of diluted H_2 [46]. Therefore, it is crucial to select optimal pretreatment and analysis conditions. The Pt dispersion of the samples investigated in this study, obtained through H_2-pulse chemisorption, displayed apparent differences. Metal dispersion of catalysts has been considered a key factor regarding catalytic activity [47-49]. Here, the $T_{50\%}$ of the Pt/AlCe-X catalysts tested under both reaction conditions, was consistently shifted to

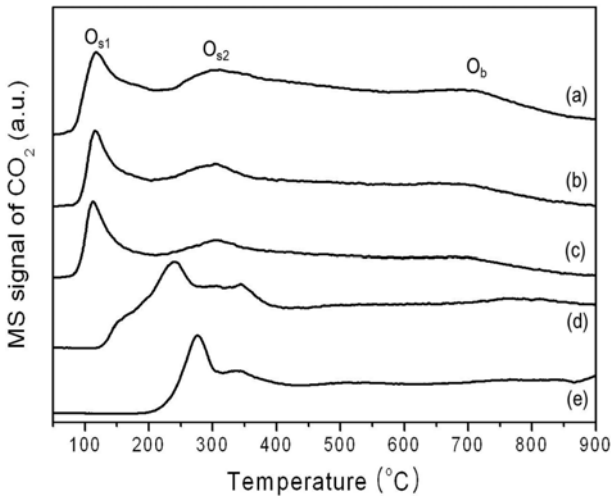

Fig. 9. CO-TPR profiles of Pt/AlCe-X catalysts; (a) X=AH, (b) PH, (c) SH, (d) PC, and (e) SC.

higher temperatures with decreases in active Pt area and Pt dispersion. Therefore, we can conclude that catalytic activity is closely related to Pt dispersion, and that the excellent catalytic behavior of the Pt/AlCe-AH catalyst could be attributed to it having the highest Pt dispersion.

The CO-TPR profiles for the Pt/AlCe-X catalysts are shown in Fig. 9. Several types of CO_2 peak were observed for all the catalysts. The low-temperature CO_2 peaks (denoted as O_{s1} and O_{s2}) observed in the range 50-200 °C, resulted from the interaction between the gas phase CO adsorbed on the Pt sites and the surface or lattice oxygen species. The O_{s1} and O_{s2} peak positions were almost the same in the catalysts prepared with hydroxide-form precipitants, indicating that these catalysts had similar reducibility and oxygen mobility [24]. The peak positions of the catalysts prepared with carbonate-form precipitants were shifted to higher temperatures than the catalysts prepared with hydroxide-form precipitants. This indicates that catalysts prepared with carbonate-form precipitants had relatively weak oxygen mobility due to the difference in the structural properties resulting from the different types of anion species of the carbonate ions on the AlCe oxide. The high-temperature peak (denoted as O_b) in the range 550-850 °C was attributed to reaction with the bulk oxygen species in the AlCe oxides. For the high-temperature peak, all catalysts showed similar reducibility, as demonstrated by the similar CO_2 formation temperature. The TPD spectra obtained after CO_2 adsorption on the Pt/AlCe-X catalysts are shown in Fig. S1. Each CO_2-TPD profile shows two desorption peaks: a low-temperature desorption peak at ~70 °C with a shoulder peak at ~150 °C, and a high-temperature peak at 350-420 °C, meaning that two types of CO_2 adsorption sites are present on the catalyst surface. The low- and high-temperature desorption peaks might be attributable to monodentate and bidendate CO_2 adsorbed on the catalyst surface, respectively [50]. The high-temperature desorption peaks were negligible compared with the low-temperature desorption peak. The adsorption capacity of CO_2 on these catalysts increased with increasing surface area, indicating that the surface density of the adsorption sites increased with surface area. In addition, the degree of basicity on the Pt/AlCe-X catalysts, estimated from the low-temperature desorption peak, decreased in the following order: Pt/AlCe-AH>Pt/AlCe-PH>Pt/AlCe-SH>Pt/AlCe-PC>Pt/AlCe-SC, and the basicity trend showed the same tendency as the catalytic activity. Although oxygen mobility is not the only factor relevant to explaining the basicity of CeO_2-based catalysts due to the presence of oxygen vacancies on this oxide, catalysts with large basicity exhibited better oxygen mobility because of the presence of unsaturated O^{2-} species on the supports [51]. Therefore, it can be speculated that the Pt/AlCe-AH catalyst which showed the best basicity of all the samples, had better oxygen mobility.

We investigated how the natures of different precipitants might affect the physicochemical properties of CeO_2-based oxide supports and their catalytic activity for CO oxidation. The supports or catalysts with high surface area could enhance the adsorption capacity of reactants and the dispersion of active metals. Catalysts prepared with hydroxide-form precipitants had higher surface areas than those prepared with carbonate-form precipitants. The Pt/AlCe-AH catalysts that exhibited the best catalytic activity in this study had a surface area of 102 $m^2 \cdot g^{-1}$. Conversely, the Pt/AlCe-SC catalyst, which exhibited the lowest catalytic activity, had a surface area of 17 $m^2 \cdot g^{-1}$. The high surface area of catalyst can facilitate the mass transfer and the adsorption of reactants; therefore, surface area can affect catalytic activity in the oxidation reaction. It has been reported that an increased surface area of catalyst could be the factor responsible for the excellent catalytic performance for CO and C_3H_8 oxidation [52]. Thus, we can deduce that catalytic performance is related somewhat to the surface area of the catalyst. For noble metal-based catalysts, the addition or presence of alkali ions could affect the electronic properties of the active noble metal species [53,54]. The surface OH group derived from the alkali metal could be formed on the Pt-OH-alkali sites on highly dispersed Pt sites, which would facilitate the formation of formate intermediates in the WGS and CO oxidation, whereas poorly dispersed Pt would inhibit the adsorption of CO. As discussed above, the Pt/AlCe-PH catalyst had greater dispersion in comparison with the Pt/AlCe-PC catalyst. Although various parameters determine catalytic activity, in relation to alkali metals, we might expect a greater promotional effect on the Pt/AlCe-PH catalyst than the Pt/AlCe-PC catalyst because of the larger amount of accessible active Pt sites.

The correlation curves between $T_{50\%}$ and the amount of CO_2 formation obtained during the CO-TPR analysis are displayed in Fig. 10. The amounts of formed CO_2 refer to the surface or lattice oxygen vacancy of the catalysts, which can be calculated by integrating the observed CO_2 peak below 200 °C during the CO-TPR runs. For the Pt/AlCe catalysts prepared by hydroxide-form precipitants, all catalysts showed similar oxygen mobility as explained above; however, the oxygen vacancy calculated from the CO_2 peak area revealed subtle differences. The oxygen vacancy decreased in the following order: Pt/AlCe-AH>Pt/AlCe-PH>Pt/AlCe-SH. In addition, the Pt/AlCe catalysts prepared with carbonate-form precipitants had a lower oxygen vacancy and poorer oxygen mobility compared with catalysts prepared with hydroxide-form precipitants. From the CO-TPR analysis, it is clear that the Pt/AlCe-AH

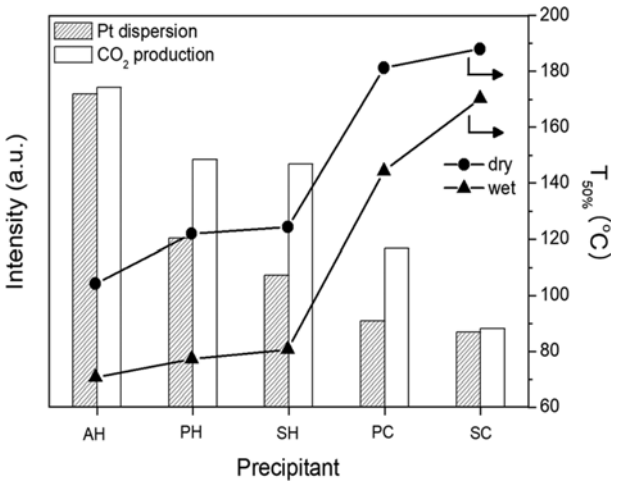

Fig. 10. $T_{50\%}$, Pt dispersion, and CO_2 quantity produced during CO-TPR of the Pt/AlCe-X catalysts with respect to precipitant.

catalyst had the greatest surface or lattice oxygen vacancies, and that the tendency of those values was parallel with catalytic activity. To sum up, with consideration of the various characterization results, we determined that precipitant nature can influence the structural properties of catalysts, e.g., Pt dispersion and oxygen vacancy/mobility, and that these values are closely related to catalytic activity in CO oxidation. In addition, NH_4OH was established as the optimal precipitant for AlCe oxide under our experimental conditions.

CONCLUSIONS

We prepared 0.1Al-0.9Ce oxides with various precipitants (NH_4OH, KOH, NaOH, K_2CO_3, and Na_2CO_3) and used as supports for Pt/0.1Al-0.9Ce catalysts. The employed precipitants affected both the structural properties of the 0.1Al-0.9Ce oxide support and the catalytic activity in CO oxidation. Among the studied catalysts, the Pt/0.1Al-0.9Ce catalyst prepared with NH_4OH showed the highest CO conversion under the given reaction conditions. Catalytic activity decreased in the following order depending on the precipitant: NH_4OH>KOH>NaOH>K_2CO_3>Na_2CO_3. The Pt/0.1Al-0.9Ce-NH_4OH catalyst was revealed to have the largest oxygen vacancy (based on the CO-TPR analysis) and the highest Pt dispersion (based on H_2-chemisorption), whereas, the catalyst prepared with Na_2CO_3 was had the lowest values. The tendencies of oxygen vacancy and Pt dispersion, depending on the precipitant, were found in good agreement with the trend toward catalytic activity. Therefore, it could be deduced that the catalytic activity of the Pt/0.1Al-0.9Ce-X catalysts was closely related to oxygen vacancy and Pt dispersion.

ACKNOWLEDGEMENT

This research was supported by Basic Science Research Program through the National Research Foundation of Korea (NRF) funded by the Ministry of Science, ICT and Future Planning (2017R1A2B3011316).

SUPPORTING INFORMATION

Additional information as noted in the text. This information is available via the Internet at http://www.springer.com/chemistry/journal/11814.

REFERENCES

1. US EPA, 2009. http://www.epa.gov/neca/roe.
2. W.-M. Miles and D. J. William, *Mol. Catal.*, **439**, 9 (2017).
3. Transportation Research Board and National Research Council, *The ongoing Challenge of Managing Carbon Monoxide Pollution in Fairbanks, Alaska*, National Academies Press, Washington DC (2002).
4. W. Lang, P. Laing, Y. Cheng, C. Hubbard and M. P. Harold, *Appl. Catal. B: Envrion.*, **218**, 430 (2017).
5. Z. Zailei, Z. Yihan, A. Hiroyuki, Z. Bin, Z. Jiaguang, Z. Maoxiang, H. Yu, T. Tsunehiro, W. Aiqin, Z. Tao and Y. Ning, *Nature Commun.*, **8**, 16100 (2017).
6. S. Royer and D. Duprez, *ChemCatChem.*, **3**, 24 (2011).
7. F. Morfin, R.-S. Nguyen, J.-L. Rousset and L. Piccolo, *Appl. Catal. B: Environ.*, **197**, 2 (2016).
8. K.-W. Jeon, D.-W. Jeong, W.-J. Jang, J.-O. Shim, H.-S. Na, H.-M. Kim, Y.-L. Lee, B.-H. Jeon, S.-H. Kim, J. W. Bae and H.-S. Roh, *Korean J. Chem. Eng.*, **33**, 1781 (2016).
9. L. Jian, W. Xiaodong and Z. Tao, *Chinese J. Catal.*, **37**, 1805 (2016).
10. S. A. Nikolaev, E. V. Golubina, I. N. Krotova, M. I. Shilina, A. V. Chistyakov and V. V. Kriventsov, *Appl. Catal. B: Environ.*, **168-169**, 303 (2015).
11. J. E. Park and E. D. Park, *Korean J. Chem. Eng.*, **31**, 1985 (2014).
12. Z. Liangpeng, L. Kongzhai, W. Hua, Y. He, Z. Xing, W. Yonggang, N. Peihong, S. Congzhi and L. Yongming, *J. Phy. Chem. C*, **121**, 12696 (2017).
13. M. Y. Kim, J. H. Park, C. H. Shin, S. W. Han and G. Seo, *Catal. Lett.*, **103**, 463 (2009).
14. S. Erdem, W. Chao, L. Michael and L. Jochen, *J. Mater. Chem. A*, **5**, 12998 (2017).
15. S. Qi, B. A. Cheney, R. Zheng, W. W. Lonergan, W. Yu and J. G. Chen, *Appl. Catal. A: Gen.*, **393**, 44 (2011).
16. L. Yang and L. Jingyue, *Ind. Eng. Chem. Res.*, **56**, 6916 (2017).
17. M. Okumura, S. Tsubota and M. Haruta, *J. Mol. Catal. A: Chem.*, **199**, 73 (2003).
18. C. Dingkai, H. Dedong, L. Jichang, Z. Liping, L. Feng, L. Jiangping, Y. Jie, W. Gengping, H. Sufang and L. Yongming, *Appl. Catal. B: Environ.*, **218**, 249 (2017).
19. D. Mukherjee, B. Govinda and B. M. Reddy, *Appl. Catal. B: Environ.*, **197**, 105 (2016).
20. S. Putla, M. H. Amin, B. M. Reddy, A. Nafady, K. A. Farhan and S. K. Bhargava, *ACS Appl. Mater. Interfaces*, **7**, 16525 (2015).
21. H. Bao, X. Chen, J. Fang and W. Huang, *Catal. Lett.*, **125**, 160 (2008).
22. J. Fan, X. Wu, X. Wu, Q. Liang, R. Ran and D. Weng, *Appl. Catal. B: Environ.*, **81**, 38 (2008).
23. S. Hosokawa, S. Imamura, S. Iwamoto and M. Inoue, *J. Eur.*

Ceram. Soc., **31**, 2463 (2011).
24. L. V. Mattos, E. R. de Oliveira, P. D. Resende, F. B. Noronha and F. B. Passos, *Catal. Today*, **77**, 245 (2002).
25. G. Del Angel, J. M. Padilla, I. Cuauhtémoc and J. Navarrete, *J. Mol. Catal. A: Chem.*, **281**, 173 (2008).
26. W.-Y. Chen, N. Li, M.-F. Luo and J.-Q. Lu, *Appl. Catal. B: Environ.*, **127**, 159 (2012).
27. N. Kakuta, N. Morishima, M. Kotobuki, T. Iwase, T. Mizushima, Y. Sato and S. Matsuura, *Appl. Surf. Sci.*, **121**, 408 (1997).
28. J.-H. Park, J. H. Cho, K. H. Cho, T. W. Lee, H. S. Han and C.-H. Shin, *Korean J. Chem. Eng.*, **29**, 1151 (2012).
29. L. Liu, F. Zhou, L. Wang, X. Qi, F. Shi and Y. Deng, *J. Catal.*, **274**, 1 (2010).
30. X. Tang, J. Chen, X. Huang, Y. Xu and W. Shen, *Appl. Catal. B: Environ.*, **81**, 115 (2008).
31. M. E. Günay and R. Yildirim, *Appl. Catal. A: Gen.*, **377**, 174 (2010).
32. R. J. Gorte, *AIChE J.*, **56**, 1126 (2010).
33. Z. Song, P. Ning, Q. Zhang, X. Liu, J. Zhang, Y. Wang, Y. Duan and Z. Huang, *J. Mol. Catal. A: Chem.*, **413**, 15 (2016).
34. L.-N. Cai, Y. Guo, A.-H. Lu, P. Branton and W. C. Li, *J. Mol. Catal. A: Chem.*, **360**, 35 (2012).
35. A. Manasilp and E. Gulari, *Appl. Catal. B: Environ.*, **37**, 17 (2002).
36. A. Parinyaswan, S. Pongstabodee and A. Luengnaruemitchai, *Int. J. Hydrogen Energy*, **31**, 1942 (2006).
37. V. Sebastian, S. Irusta, R. Mallada and J. Santamaria, *Appl. Catal. A: Gen.*, **366**, 242 (2009).
38. L. Z. Linganiso, G. Jacobs, K. G. Azzam, U. M. Graham, B. H. Davis, D. C. Cronauer, A. J. Kropf and C. L. Marshall, *Appl. Catal. A: Gen.*, **394**, 105 (2011).
39. J. L. Herberg, R. S. Maxwell and E. H. Majzoub, *J. Alloy. Compd.*, **417**, 39 (2006).
40. J.-H. Park, J. H. Cho, S. E. Kang, K. H. Cho, T. W. Lee, H. S. Han and C.-H. Shin, *Korean J. Chem. Eng.*, **30**, 598 (2013).
41. J. H. Kwak, J. Hu, D. Mei, C.-W. Yi, D. H. Kim, C. H. F. Peden, L. F. Allard and J. Szanyi, *Science*, **325**, 1670 (2009).
42. S. Li, H. Qin, R. Zuo and Z. Bai, *Appl. Surf. Sci.*, **353**, 643 (2015).
43. R. Sasikala, V. Sudarsan and S. K. Kulshreshtha, *J. Solid State Chem.*, **169**, 113 (2002).
44. J. H. Kwak, J. Z. Hu, D. H. Kim, J. Szanyi and C. H. F. Peden, *J. Catal.*, **251**, 189 (2007).
45. C. Dong, X. Li, A. Wang and Y. Chen, *Catal. Today*, **207**, 124 (2017).
46. T. Takeguchi, S, Manabe, R. Kikuchi, K. Eguchi, T. Kanazwa, S. Matsumoto and W. Ueda, *Appl. Catal. A: Gen.*, **293**, 91 (2005).
47. P. Chantaravitoon, S. Chavadej and J. Schwank, *Chem. Eng. J.*, **98**, 99 (2004).
48. C. L. Pieck, C. R. Vera, J. M. Parera, G. N. Giménez, L. R. Serra, L. S. Carvalho and M. C. Rangel, *Catal. Today*, **107-108**, 637 (2005).
49. H. Iida, K. Kondo and A. Igarashi, *Catal. Commun.*, **7**, 240 (2006).
50. M. F. Luo, Y. J. Zhong, B. Zhu, X. X. Yuan and X. M. Zheng, *Appl. Surf. Sci.*, **115**, 185 (1997).
51. D. Martin and D. Duprez, *J. Phys. Chem.*, **100**, 9429 (1996).
52. B. Zhao, R. Ran, L. Sun, Z. Yang, X. Wu and D. Weng, *Catal. Commun.*, **105**, 26 (2018).
53. X. Yang, X. Su, X. Chen, H. Duan, B. Liang, Q. Liu, X. Liu, Y. Ren, Y. Huang and T. Zhang, *Appl. Catal. B: Environ.*, **216**, 95 (2017).
54. Z. Yanping, P. Danny, S. Rui, D. Weiling, F. Peter, U. N. Anand, P. Guowen, A. H. Jeffrey, C. B. David, S. Howard, M. Manos and F.-S. Maria, *Science*, **329**, 1633 (2010).

Supporting Information

Low-temperature CO oxidation of $Pt/Al_{0.1}Ce_{0.9}O_x$ catalysts: Effects of supports prepared with different precipitants

Jung-Hyun Park*, Hyeryeung Noh, Tae-Sun Chang*, and Chae-Ho Shin**,†**

*Greenhouse Gas Resources Research Group, Korea Research Institute of Chemical Technology, Daejeon 34114, Korea
**Department of Chemical Engineering, Chungbuk National University, Cheongju, Chungbuk 28644, Korea
(*Received 28 August 2017 • accepted 12 December 2017*)

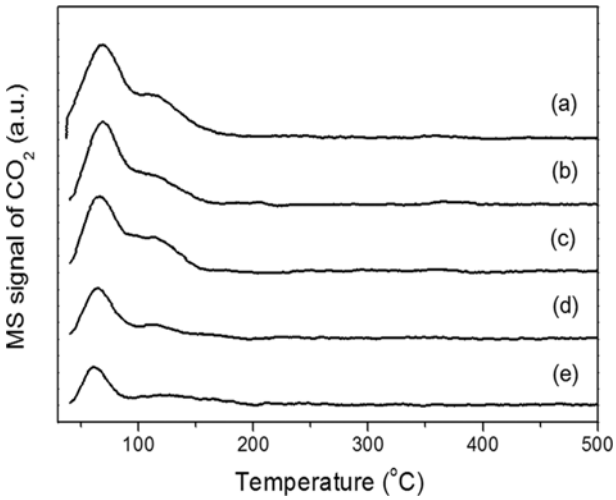

Fig. S1. CO_2-TPD profiles of Pt/AlCe-X catalysts: (a) X=AH, (b) PH, (c) SH, (d) PC, and (e) SC.